Volume 17 | Number 47 | 21 December 2019 | Pages 9969–10110

Organic & Biomolecular Chemistry

rsc.li/obc

ISSN 1477-0520

ROYAL SOCIETY OF CHEMISTRY | Celebrating IYPT 2019

PAPER

Michael Watkinson *et al.*

An alternative modular 'click-S_NAr-click' approach to develop subcellular localised fluorescent probes to image mobile Zn^{2+}

Organic & Biomolecular Chemistry

PAPER

View Article Online
View Journal | View Issue

Cite this: *Org. Biomol. Chem.*, 2019, **17**, 10013

An alternative modular 'click-S_NAr-click' approach to develop subcellular localised fluorescent probes to image mobile Zn^{2+} †

Le Fang, [a] Giuseppe Trigiante,[b] Rachel Crespo-Otero, [a] Michael P. Philpott,[b] Christopher R. Jones [a] and Michael Watkinson *[c]

Received 23rd August 2019,
Accepted 8th October 2019

DOI: 10.1039/c9ob01855g

rsc.li/obc

Zn^{2+} is involved in a number of biological processes and its wide-ranging roles at the subcellular level, especially in specific organelles, have not yet been fully established due to a lack of tools to image it effectively. We report a new and efficient modular double 'click' approach towards a range of sub-cellular localised probes for mobile zinc. Through this methodology, endoplasmic reticulum, mitochondria and lysosome localised probes were successfully prepared which show good fluorescence responses to mobile Zn^{2+} *in vitro* and *in cellulo* whilst a non-targeting probe was synthesized as a control. The methodology appears to have wide-utility for the generation of sub-cellular localised probes by incorporating specific organelle targeting vectors for mobile Zn^{2+} imaging.

Introduction

Zinc, as the second most abundant d-block metal in the human body, plays an extremely important role in a wide range of biological processes, such as brain function and pathology,[1,2] immune function,[3,4] gene transcription,[5,6] and mammalian reproduction.[7] Due to this, problems with zinc homeostasis are associated with many diseases, including Alzheimer's disease,[8] prostate cancer,[9,10] type 2 diabetes,[11] and ischemic stroke.[12] Though most of the zinc is in bound forms, there exist mobile pools of zinc that play a critical role in a range of cellular processes and its biological trafficking and control is performed by a complex array of transporter proteins.[13,14] Variation in these tightly regulated mobile zinc levels adversely affects a number of cellular processes. For example, it is known that the dysregulation of zinc transporters or zinc deficiency in the endoplasmic reticulum (ER) causes ER stress and this activates the unfolded protein response (UPR).[15–17] In addition, Zn^{2+} is closely associated with the mitochondrial respiratory chain and this organelle is also involved in intracellular Zn^{2+} transportation and storage.[18–20] The influx of hydrogen peroxide also results in a rapid release of Zn^{2+} that accumulates in the lysosome, causing lysosomal membrane permeabilization (LMP)[21] inducing hippocampal neuronal death, which is related to various neurodegenerative diseases.[2,22] Therefore, a comprehensive understanding of the distribution, uptake and trafficking of mobile Zn^{2+} in biological systems, especially at the sub-cellular level is essential for the development of a fundamental understanding of its role in the array of biological processes it is associated with.

Small molecule fluorescent probes have many advantages as tools to image mobile zinc such as their high sensitivity and selectivity, low toxicity, and good photophysical properties. Consequently they have been widely used to investigate biological events involving mobile zinc.[23–27] However, a failure to control the probes' sub-cellular location limits their utility somewhat. In the last decade, there have been extensive efforts in the development of probes to detect mobile zinc in specific cellular space, such as the extracellular plasma membrane,[28–31] mitochondria,[32–35] lysosome,[36–39] ER[40,41] and the Golgi apparatus.[42,43] Whilst some success has been achieved through adventitious localisation, probe localisation in specific organelles through the inclusion of targeting vectors has proven to be the most effective and reliable strategy. For example, the triphenylphosphonium salt (TPP)[32,44,45] has been demonstrated to target the mitochondria effectively, whilst basic ethylenediamine[36] or morpholine[38,39,46] groups have been used to target lysosomal space. Whilst this strategy has not been as widely explored in ER-localized fluorescent Zn^{2+} probes a number of recent reports have appeared in which the methyl sulfonamide group has been used as a tar-

[a]*The Joseph Priestley Building, School of Biological and Chemical Science, Queen Mary University of London, Mile End Road, London, E1 4NS, UK*
[b]*Centre for Cutaneous Research, Institute of Cell and Molecular Science, Barts and The London School of Medicine and Dentistry, Queen Mary University of London, London E1 2AT, UK*
[c]*The Lennard-Jones Laboratories, School of Chemical and Physical Science, Keele University, ST5 5BG, UK. E-mail: m.watkinson@keele.ac.uk*
†Electronic supplementary information (ESI) available. See DOI: 10.1039/c9ob01855g

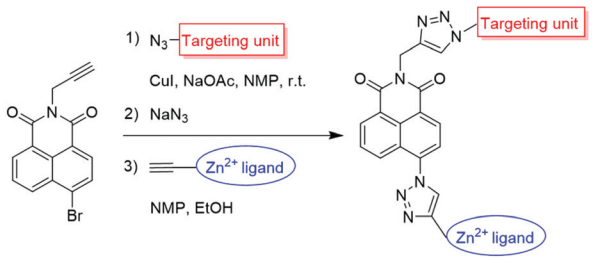

Fig. 1 The 'top to bottom' methodology originally reported.[51,52]

geting unit to visualize hydrogen peroxide,[47] methylglyoxal,[48] hypochlorite[49] and hydrogen sulfide[50] in the ER.

Previously we have reported a modular 'click' synthetic methodology to produce an array of fluorescent probes for imaging of zinc at specific cellular targets (see Fig. 1),[51,52] whilst others have also used 'click' methodology to good effect in naphthalimide-based probes.[53,54] However, this methodology, based on a 'top to bottom' double click process can be hampered somewhat by the final synthetic step, which can be a slow, moderately low yielding reaction and can also lead to the unwanted formation of an aniline by-product that is difficult to remove. This is unattractive if the targeting unit is either expensive or requires complex multi-step synthesis. Therefore, we sought to develop an alternative approach to ameliorate these issues and were attracted by a modular strategy involving a 'bottom to top' double click reaction methodology, which would have the advantage that high value organelle targeting vectors could be introduced in the last synthetic step, which is generally fast and high yielding.

Results and discussion

Synthesis and characterisation

The precursors **1**,[55] **2**,[56] **4**,[57] **5**,[51] **6**[51] were all synthesized according to reported procedures. The conversion of azide **1**, to alkyne **3** (Scheme 1), was performed in a one-pot reaction because the intermediate formed after the 'click' reaction could not be readily extracted from the aqueous layer. It proved expedient to simply follow this step by the direct addition of propargylamine to the reaction mixture to give **3** in a moderate yield. With alkyne **3** and the range of different organelle targeting azides **4–6** in hand, the top 'click' reactions were performed successfully in moderate to good yields to produce the different organelle targeting probes **7–9**. As a control, the non-targeting probe **10** (R^4 = Et) was also prepared as reported in 93% yield.[58] All products were satisfactorily characterized by ^{1}H, ^{13}C NMR and IR spectroscopies as well as high-resolution mass spectrometry (see ESI†).

Photophysical properties

Fluorescence titrations of the different probes with Zn^{2+} were undertaken to show their Zn^{2+} response. As shown in Fig. 2, addition of Zn^{2+} results in the fluorescence intensity of probe **7** increasing gradually, until a maximal 10-fold increase was observed; a similar response was observed in the other three

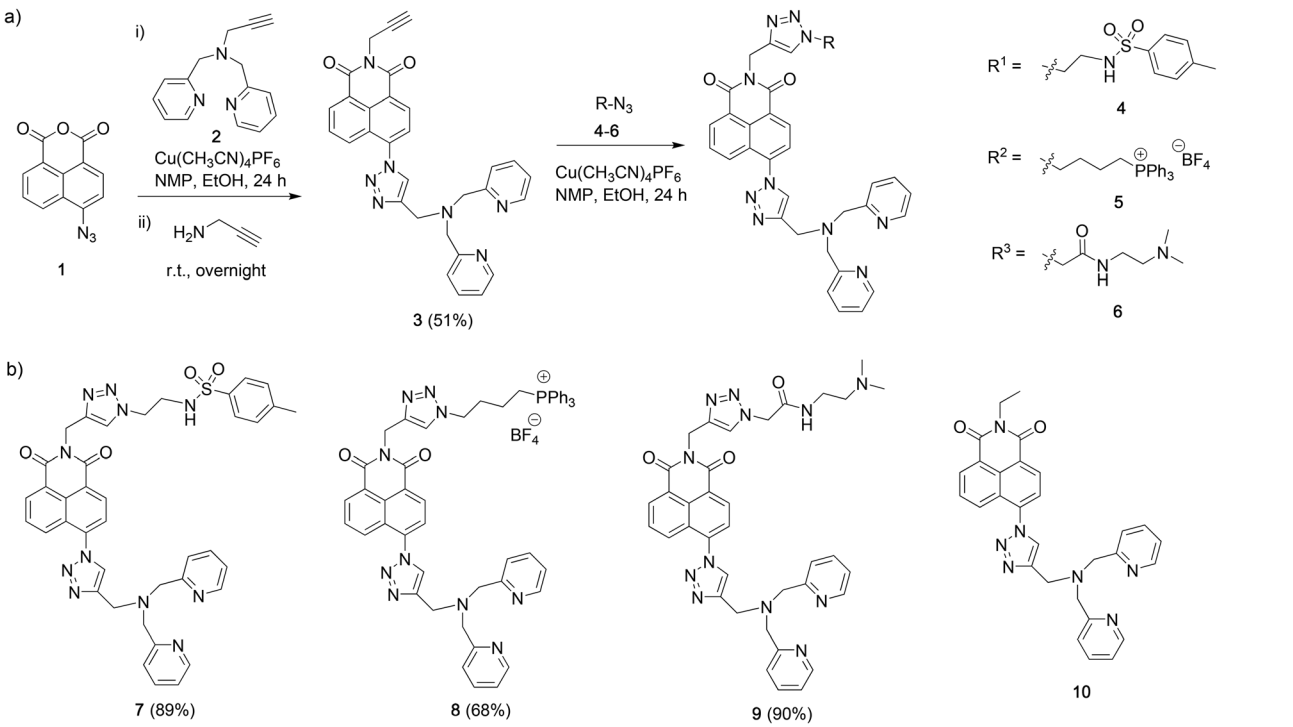

Scheme 1 a) The new 'bottom to top' modular synthetic route towards the sub-cellular targeting Zn^{2+} probes; (b) the structures of ER probe (**7**), mitochondria probe (**8**), lysosome probe (**9**) and non-targeting probe (**10**).

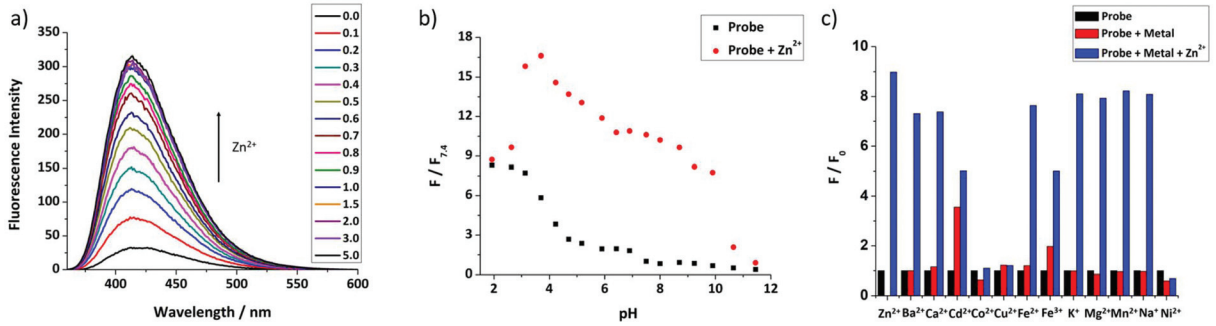

Fig. 2 (a) The fluorescence response of **7** (50 μM) to different equivalents of $ZnCl_2$; (b) the pH profile of **7** (50 μM, black dots) and its complex with 1 equivalent Zn^{2+} (red dots); (c) metal ion selectivity of **7**. Average normalized fluorescence intensities for **7** (50 μM) (black bars), after addition of 5 equivalents of various cations (red bars), followed by addition of 1 equivalent $ZnCl_2$ (blue bars). (For all tests, the solution is 0.01 mM HEPES buffer with 1% DMSO, pH = 7.4 except pH profile, λ_{ex} = 346 nm, λ_{em} = 414 nm, slit width: 5/2.5 nm.)

probes (shown in Fig. S5–S7, ESI†). The Job's plots of the probes (Fig. S8–S11, ESI†) revealed the expected 1 : 1 binding stoichiometry with Zn^{2+}. Dissociation constants, K_d, were evaluated from non-linear curve fitting analysis (Fig. S12–S15, ESI†) of the data obtained from the fluorescence titrations of different concentration probes in a competitive system with EGTA (ethylene glycol-bis(β-aminoethyl ether)-*N*,*N*,*N*′,*N*′-tetraacetic acid) and the results given in Table S1.† The best fitting for all probes was observed at 0.01 μM and K_d values were determined to be 2.83 ± 0.11 nM for **7**, 3.44 ± 0.22 nM for **8**, 3.68 ± 0.26 nM for **9** and 3.24 ± 0.20 nM for **10**, which are consistent and comparable to reported values for this chelate.[32,59] The detection limit was calculated based on the fluorescence titration data through the method reported[60,61] and was determined to be 48 pM for **7**, 99 pM for **8**, 51 pM for **9** and 47 pM for **10**.

The fluorescence quantum yield was measured using anthracene as a standard (Φ = 0.27 in ethanol) and linear plots of probes **7**–**10** and their complexes with one equivalent of Zn^{2+} are shown (Fig. S20–S23, ESI†). The calculated quantum yields are listed (Table S2, ESI†) and shows that the targeting units reduce the probes' quantum yields significantly, compared to that of **10**, with no targeting unit, presumably due to the increased access to non-radiative pathways that are available in the larger molecular structures.

The pH-dependent fluorescence response was measured to show that all probes have fluorescence responses to Zn^{2+} in the biologically relevant pH range. As shown in Fig. 2b, probe **7** shows a good switch on response to Zn^{2+} over a wide pH range 3.0–10.0, the same results were broadly observed for probes **8**–**10** (Fig. S24–S26, ESI†), as expected due to the identical metal-chelating motif. The fluorescence intensity of all probes increased in an acidic environment, however, compared to the other three probes, **7** and its complex were significantly brighter. Sessler *et al.* explained this behaviour based on a PET mechanism,[39] however Veale and Gunnlaugasson have previously suggested that this is unlikely because the PET quenching from groups connected *via* the imide moiety is normally prevented.[62] It therefore seems more likely that the differences in emission observed at different pH values are due to the presence of different species formed by the protonation of the tertiary amine or by the deprotonation of coordinated water. Given the range of pH observed in different organelles and the cytoplasm (*i.e.* the pH is about 7.2 in ER and cytoplasm, 8 in the mitochondria and around 5 in the lysosome), all probes should display a response to mobile Zn^{2+} *in cellulo*. By integrating the intensity of the fluorescence emission spectra against pH (Fig. S27–S30, ESI†) for different probes their apparent pK_a values were determined through non-linear curve fitting (eqn (S4), ESI†).

The selectivity of probes **7**–**10** was investigated in the presence of a range of other biologically relevant cations. From Fig. 2c and Fig. S31–S33 (ESI†), it can be seen that all probes display similar behaviour, which is to be expected given they contain the same metal binding motif. The fluorescence did not show an obvious increase after addition of 5 equivalents of other cations, except for the stereoelectronic isostere Cd^{2+}, which is not concerning since it is not a biologically relevant analyte. Subsequent addition of 1 equivalent of Zn^{2+} resulted in recovery of a fluorescence response for most cations, however for Co^{2+}, Cu^{2+} and Ni^{2+} fluorescence was still quenched, but as they essentially exist in bound forms in biology, rather than the free cations tested here, this should not be problematical. Therefore, the results above suggest that all probes should have a selective response to mobile Zn^{2+} *in celluo*.

NMR titration of 10 with Zn^{2+}

In order to study the binding behaviour between **10** and Zn^{2+}, a ^{1}H NMR titration with different equivalents Zn^{2+} was performed (see Fig. S34, ESI†). From Fig. 3 and Fig. S35 (see ESI†), it can be seen that protons H_{c-g} are largely unaffected, while H_{l-n}, H_h and $H_{i,j}$ have significant downfield shifts after binding with Zn^{2+}, this indicates that the ligand *N*,*N*-di-(2-picolyl)ethylenediamine (DPEN) and the triazole are involved in metal binding. This result is consistent with the behaviour observed by single crystal X-ray diffraction in related structures[63,64] as well as recent DFT calculations.[52]

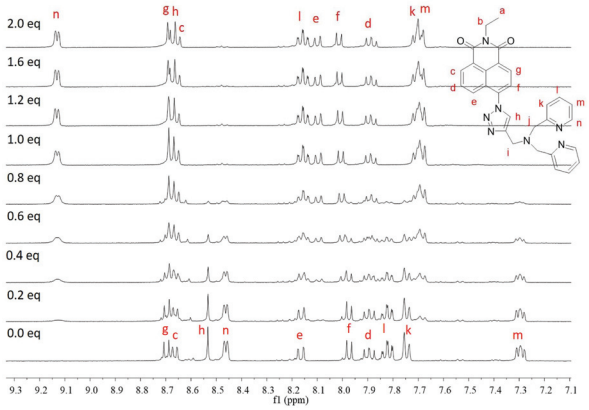

Fig. 3 The aromatic region of the ^{1}H NMR spectra of probe **10** (5 mM) with different equivalents of $ZnCl_2$ in CD_3OD.

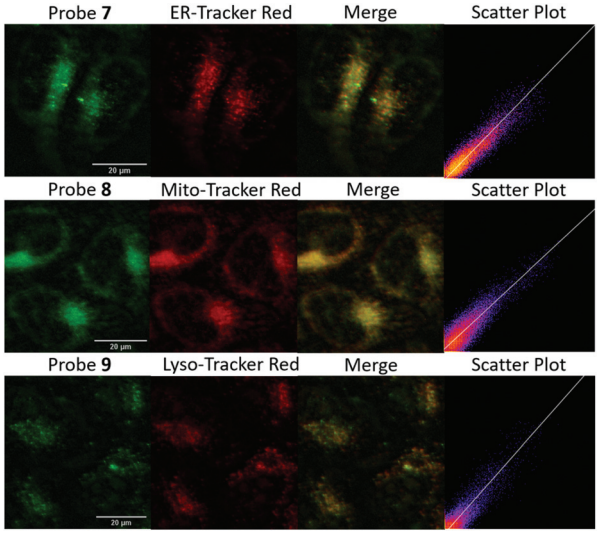

Fig. 4 The colocalization images of HeLa cells incubated with **7–9** (20 μM, GFP filter: λ_{ex} = 470/30 nm, λ_{em} = 530/50 nm) and commercial organelle tracker red dyes (RFP filter: λ_{ex} = 530/40 nm, λ_{em} = 605/55 nm). (Scale bars = 20 μm.)

DFT calculations

In addition to the ^{1}H NMR titration, DFT calculations were also undertaken to study the association between probes and Zn^{2+}. The optimised structures of the complexes of **7–10** with 1 equivalent Zn^{2+} (Fig. S36–S39, ESI†) also show the nitrogen atoms in the triazoles adjacent to the DPEN ligand are involved in binding with Zn^{2+}, in addition to those of the DPEN ligands.

TDDFT studies were also undertaken to understand the excitation and emission profiles of probes **7–10**. The results of calculated absorption energy from ground state S_0 to the excited state S_1, and the emission energy were in agreement with the experimental data (Tables S3–S6, ESI†). There was also nearly no difference among the different probes, showing that the targeting groups have negligible effects on the Zn^{2+} association and photophysical properties, other than quantum yields, which is consistent with the experimental data above.

In keeping with our previous reports,[52,65] the S_1–S_0 electron density transition (Fig. S40–S43, ESI†) of all probes is mainly localised on the naphthalimide moiety and the vicinal triazole, and there is only a slight decrease of electron density on the triazole when it is involved in complex formation and the oscillator strength is not significantly affected. Therefore, the enhancement of emissive behaviour of the complexes should be related to a reduced decay through nonradiative pathways after complexation with Zn^{2+}. The stabilisation of the complex hinders large amplitude vibrations in the vicinity of the fluorophore hampering the access to nonradiative mechanisms and increasing the quantum yield of emission. The restriction of intramolecular rotations can also hinder the access to low energy conical intersections associated with ultrafast decay to the ground state. The role of these mechanisms in contrast to PET has recently been highlighted in the literature.[66,67]

Subcellular localisation studies

As probes **7–10** show excellent photophysical properties *in vitro*, we assessed their suitability for imaging Zn^{2+} *in cellulo*. Firstly, the innate toxicity of all probes was measured through an alamarBlue cell viability assay. After 24 hours' incubation with probes **7–10**, the HeLa cells' viability (Fig. S44–S47, ESI†) did not show an obvious decrease with increasing probe concentration from 0 to 50 μM, indicating that the probes have no toxicity to cells.

Co-localisation experiments were undertaken to confirm the probes' subcellular targeting ability. HeLa cells were co-incubated with probes and organelle tracking dyes, as shown in Fig. 4, probe **7** has an excellent co-localisation with ER-tracker red with a Pearson's correlation coefficient of 0.88, and its dispersion in the ER and other organelles (Fig. S48, ESI†) compares well with recent reports.[48] Probes **8** and **9** also displayed good co-localisation with Mito-tracker red and Lyso-tracker red (Pearson's coefficients of 0.93 and 0.86 respectively, see Fig. 4 and Fig. S49, S50, ESI†). In contrast, control probe **10**, which has no targeting group, was widely distributed in all three organelles (Fig. S51, ESI†). Therefore, we can conclude that probes **7–9**, which incorporate different organelle targeting groups, have the expected organelle localisation ability.

Zn^{2+} fluorescence response in cells

As all probes displayed organelle targeting behaviour, their fluorescence response to increased levels of cellular Zn^{2+} was measured. As shown in Fig. 5a, the fluorescence of probe **7** in the ER can be observed, and after the addition of zinc pyrithione, a membrane permeable zinc source, the fluorescence intensity increased considerably. However, the addition of *N*,*N*,*N*′,*N*′-tetrakis(2-pyridinylmethyl)-1,2-ethanediamine (TPEN), a strong chelator of mobile Zn^{2+}, caused almost complete quenching of the fluorescence. Similar results were obtained for probe **8–10** (Fig. S52–S54, ESI†), indicating that all probes display a clear fluorescence response to mobile Zn^{2+} in cells and the fluorescence intensity read from the cells for each probe is shown in Fig. 5b.

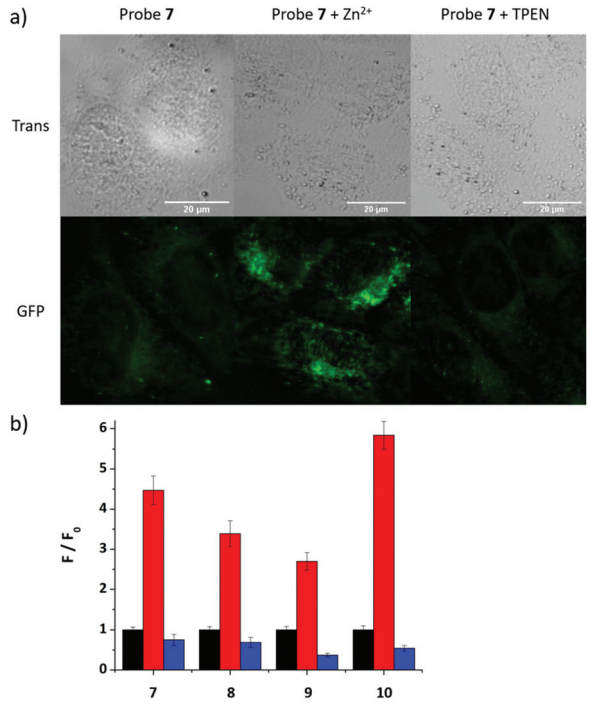

Fig. 5 (a) Fluorescence microscopy images of HeLa cells treated with **7** (20 μM), **7** (20 μM) with zinc pyrithione (100 μM), and **7** (20 μM) with TPEN (100 μM) (scale bars = 20 μm); (b) the fluorescence intensity (F) of probes in HeLa cells with zinc pyrithione (red bars) or TPEN (blue bars) relative to the intensity of the probe alone (F_0, black bars, normalised to 1).

Conclusions

In conclusion, we have developed a new modular 'bottom to top' click approach to synthesize subcellular localised probes by incorporating organelle targeting vectors in the last step click reaction, which is an effective and efficient method to prepare an array of different organelle targeting Zn^{2+} probes. Three probes **7–9** have been successfully prepared through this approach, and have been proven to localise in the ER, mitochondria and lysosome, and all display a good fluorescence response to Zn^{2+} *in vitro* and *in cellulo*. We believe that these probes have significant potential to be applied in the imaging of mobile Zn^{2+} related biological processes in these organelles and that through this method, other sub-cellular targeting mobile Zn^{2+} probes can be developed to satisfy the imaging demands of other specific cellular locations.

Experimental

6-(4-((Bis(pyridin-2-ylmethyl)amino)methyl)-1*H*-1,2,3-triazol-1-yl)-2-(prop-2-yn-1-yl)-1*H*-benzo[*de*]isoquinoline-1,3(2*H*)-dione (3)

Under a nitrogen atmosphere, azide **1** (120 mg, 0.500 mmol), alkyne **2** (119 mg, 0.500 mmol), and tetrakis(acetonitrile) copper(I) hexafluorophosphate (55.9 mg, 0.150 mmol), were added to a mixture of 1-methyl-2-pyrrolidinone (NMP, 2.0 mL) and EtOH (2.0 mL). The flask was covered with aluminium foil and the mixture was stirred at room temperature for 24 h, after the starting materials were consumed, the propargylamide (45.0 μL, 0.700 mmol) was added and the mixture was stirred at room temperature for 16 hours. After the reaction was complete, saturated EDTA in 17% $NH_3{\cdot}H_2O$ (50.0 mL) was added and the precipitate was collected by filtration, washed with water (30.0 mL). The crude product was purified by column chromatography on silica gel (eluent CH_2Cl_2 : MeOH = 20 : 1) to give **3** (131 mg, 51%) as a brown oil. ^{1}H NMR (400 MHz, $CDCl_3$) δ 8.79–8.73 (m, 2H), 8.57 (d, 2H, J = 4.2), 8.32 (dd, 1H, J = 8.6, 0.9), 8.17 (s, 1H), 7.88–7.82 (m, 2H), 7.72–7.66 (m, 2H), 7.63–7.57 (m, 2H), 7.21–7.15 (m, 2H), 5.00 (d, 2H, J = 2.4), 4.09 (s, 2H), 3.97 (s, 4H), 2.23 (t, 1H, J = 2.4). ^{13}C NMR (101 MHz, $CDCl_3$) δ 163.0, 162.5, 159.0, 149.3, 145.1, 138.8, 136.8, 135.8, 132.7, 131.2, 130.3, 129.3, 128.7, 126.6, 125.8, 123.6, 123.5, 122.7, 122.4, 78.3, 71.0, 59.9, 48.6, 29.8. IR: (ν_{max}/cm^{-1}) 1744, 1707, 1665, 1581, 1483, 1378, 1232, 1040, 845, 782, 754. HR-NSI MS (m/z) $[M + Na]^+$ calcd for $C_{30}H_{23}N_7O_2Na$ 536.1805, found 536.1796.

General procedure of top click reaction

Under an atmosphere of nitrogen, alkyne **3** (51.4 mg, 0.100 mmol) and azide **4–6** (0.100 mmol) were dissolved in the mixture of NMP (1.0 mL) and EtOH (1.0 mL), tetrakis(acetonitrile)copper(I) hexafluorophosphate (7.5 mg, 0.020 mmol) was added. The mixture was stirred at room temperature for 24 hours. After the reaction had finished, saturated EDTA in 17% $NH_3{\cdot}H_2O$ (10.0 mL) was poured into the mixture and the precipitate that formed was collected by filtration, and washed with water (30.0 mL). The crude product was purified by flash chromatography on silica gel (eluent: CH_2Cl_2/MeOH 20 : 1) to give product **7–9** as brown solids.

N-(2-(1-((6-(4-((Bis(pyridin-2-ylmethyl)amino)methyl)-1*H*-1,2,3-triazol-1-yl)-1,3-dioxo-1*H*-benzo[*de*]isoquinolin-2(3*H*)-yl)methyl)-1*H*-1,2,3-triazol-4-yl)ethyl)-4-methylbenzenesulfonamide (7)

(67.1 mg, 89%, M.p. 103–107 °C). ^{1}H NMR (400 MHz, $CDCl_3$) δ 8.72–8.67 (m, 2H), 8.55 (d, 2H, J = 4.1), 8.28 (d, 1H, J = 7.8), 8.17 (s, 1H), 7.85–7.78 (m, 2H), 7.72–7.65 (m, 5H), 7.63–7.59 (m, 2H), 7.29 (d, 2H, J = 8.0), 7.21–7.15 (m, 2H), 5.50 (s, 2H), 5.18–5.09 (m, 1H), 4.45–4.38 (m, 2H), 4.08 (s, 2H), 3.96 (s, 4H), 3.51–3.45 (m, 2H), 2.41 (s, 3H). ^{13}C NMR (101 MHz, $CDCl_3$) δ 163.4, 162.9, 159.1, 149.2, 145.0, 143.8, 143.2, 138.5, 136.9, 136.8, 132.5, 131.1, 130.1, 129.9, 129.0, 128.6, 127.1, 126.3, 125.8, 124.9, 123.6, 123.5, 123.3, 122.6, 122.4, 59.9, 50.3, 48.6, 42.7, 35.4, 21.6. IR: (ν_{max}/cm^{-1}) 3073, 1704, 1662, 1589, 1432, 1329, 1233, 1157, 1041, 996, 786, 660. HR-NSI MS (m/z) $[M + H]^+$ calcd for $C_{39}H_{36}N_{11}O_4S$ 754.2667, found 754.2662.

(4-(1-((6-(4-((Bis(pyridin-2-ylmethyl)amino)methyl)-1*H*-1,2,3-triazol-1-yl)-1,3-dioxo-1*H*-benzo[*de*]isoquinolin-2(3*H*)-yl)methyl)-1*H*-1,2,3-triazol-4-yl)butyl)triphenylphosphonium tetrafluoroborate (8)

(130 mg, 68%, M.p. 131–135 °C). ^{1}H NMR (400 MHz, $CDCl_3$) δ 8.58–8.50 (m, 2H), 8.47 (d, 2H, J = 4.3), 8.22 (s, 1H), 8.17 (d, 1H, J = 8.5), 7.78–7.74 (m, 2H), 7.72–7.57 (m, 20H), 7.15–7.07

(m, 2H), 5.34 (s, 2H), 4.34 (t, 2H, J = 6.3), 4.01 (s, 2H), 3.90 (s, 4H), 3.35–3.24 (m, 2H), 2.17–2.04 (m, 2H), 1.62–1.49 (m, 2H). ^{13}C NMR (101 MHz, $CDCl_3$) δ 163.3, 162.7, 159.0, 149.0, 145.1, 143.3, 138.4, 136.7, 135.1 (d, J = 2.8), 133.4 (d, J = 10.0), 132.3, 131.0, 130.5 (d, J = 12.6), 129.9, 129.0, 128.4, 126.3, 125.8, 123.6, 123.5, 123.4, 123.3, 122.6, 122.2, 117.8 (d, J = 85.8), 59.8, 53.5, 48.6, 35.5, 29.9 (d, J = 17.3), 21.1 (d, J = 53.5), 19.2. ^{31}P NMR (162 MHz, $CDCl_3$) δ 23.91. ^{19}F NMR (377 MHz, $CDCl_3$) δ −151.75. IR: (ν_{max}/cm^{-1}) 3067, 1738, 1585, 1436, 1366, 1232, 1112, 1037, 785, 689. HR-NSI MS (m/z) $[M - BF_4]^+$ calcd for $C_{52}H_{46}N_{10}O_2P$ 873.3537, found 873.3544.

2-(1-((6-(4-((Bis(pyridin-2-ylmethyl)amino)methyl)-1*H*-1,2,3-triazol-1-yl)-1,3-dioxo-1*H*-benzo[*de*]isoquinolin-2(3*H*)-yl)methyl)-1*H*-1,2,3-triazol-4-yl)-*N*-(2-(dimethylamino)ethyl)acetamide (9)

(92.4 mg, 90%, M.p. 113–117 °C). ^{1}H NMR (400 MHz, $CDCl_3$) δ 8.71–7.64 (m, 2H), 8.53 (d, 2H, J = 4.7), 8.26 (d, 1H, J = 8.6), 8.17 (s, 1H), 7.86 (s, 1H), 7.83–7.76 (m, 2H), 7.70–7.63 (m, 2H), 7.59 (d, 2H, J = 7.8), 7.18–7.12 (m, 2H), 6.70–6.58 (bs, 1H), 5.52 (s, 2H), 5.00 (s, 2H), 4.06 (s, 2H), 3.94 (s, 4H), 3.32–3.23 (m, 2H), 2.34 (t, 2H, J = 6.1), 2.13 (s, 6H). ^{13}C NMR (101 MHz, $CDCl_3$) δ 165.1, 163.3, 162.8, 159.0, 149.2, 145.0, 143.6, 138.5, 136.6, 132.4, 131.0, 130.0, 129.1, 128.5, 126.3, 125.7, 125.1, 123.4 (overlapping signals), 122.6, 122.2, 59.8, 57.4, 52.9, 48.5, 45.0, 37.2, 35.4. IR: (ν_{max}/cm^{-1}) 3128, 1610, 1551, 1473, 1428, 1366, 1231, 1038, 810, 782. HR-NSI MS (m/z) $[M + H]^+$ calcd for $C_{36}H_{37}N_{12}O_3$ 685.3106, found 685.3104.

6-(4-((Bis(pyridin-2-ylmethyl)amino)methyl)-1*H*-1,2,3-triazol-1-yl)-2-ethyl-1*H*-benzo[*de*]isoquinoline-1,3(2*H*)-dione (10)

Under a nitrogen atmosphere, 4-azido-*N*-ethyl-1,8-naphthalimide **S5** (0.160 g, 0.62 mmol) and alkyne **2** (0.150 g, 0.62 mmol) were dissolved in a mixture of NMP (6.2 mL) and EtOH (6.2 mL). To this mixture tetrakis(acetonitrile)copper(I) hexafluorophosphate (45.0 mg, 0.12 mmol) was added and stirred at room temperature for 24 hours. After the reaction was complete, saturated EDTA in 17% $NH_3{\cdot}H_2O$ (20.0 mL) was poured into the mixture and the precipitate that formed was collected by filtration, then washed with water (30.0 mL). This crude product was purified by flash chromatography (eluent: DCM/MeOH 20 : 1) to give **10** (0.290 g, 93%, M.p. 93–97 °C) as a brown solid. ^{1}H NMR (400 MHz, $CDCl_3$) δ 8.67–8.60 (m, 2H), 8.48 (dd, 2H, J = 4.9, 0.8), 8.19 (dd, 1H, J = 8.6, 1.0), 8.11 (s, 1H), 7.78–7.71 (m, 2H), 7.65–7.58 (m, 2H), 7.54 (d, 2H, J = 7.8), 7.13–7.07 (m, 2H), 4.20 (q, 2H, J = 7.1), 4.01 (s, 2H), 3.89 (s, 4H), 1.29 (t, 3H, J = 7.1). ^{13}C NMR (101 MHz, $CDCl_3$) δ 163.4, 162.9, 158.9, 149.1, 144.9, 138.2, 136.6, 132.0, 130.6, 129.5, 128.9, 128.5, 126.3, 125.7, 125.5, 123.7, 123.4, 122.9, 122.2, 59.8, 48.4, 35.7, 13.3. IR: (ν_{max}/cm^{-1}) 3196, 1703, 1611, 1551, 1473, 1427, 1365, 1230, 1119, 1037, 950, 726. HR-NSI MS (m/z) $[M + H]^+$ calcd for $C_{29}H_{26}N_7O_2$ 504.2142, found 504.2134.

Conflicts of interest

There are no conflicts to declare.

Acknowledgements

We acknowledge the EPSRC National Mass Spectrometry Service, University of Wales, Swansea for the provision of high-resolution mass spectrometry. DFT calculations were performed on the QMUL Apocrita facility. LF is grateful to the Chinese Scholarship Council for the provision of a PhD studentship.

Notes and references

1 S. L. Sensi, P. Paoletti, A. I. Bush and I. Sekler, *Nat. Rev. Neurosci.*, 2009, **10**, 780–791.
2 S. L. Sensi, P. Paoletti, J.-Y. Koh, E. Aizenman, A. I. Bush and M. Hershfinkel, *J. Neurosci.*, 2011, **31**, 16076–16085.
3 A. S. Prasad, *Mol. Med.*, 2008, **14**, 353–357.
4 P. Bonaventura, G. Benedetti, F. Albarède and P. Miossec, *Autoimmun. Rev.*, 2015, **14**, 277–285.
5 R. K. Blanchard, J. B. Moore, C. L. Green and R. J. Cousins, *Proc. Natl. Acad. Sci. U. S. A.*, 2002, **98**, 13507–13513.
6 K. A. Jackson, R. A. Valentine, L. J. Coneyworth, J. C. Mathers and D. Ford, *Biochem. Soc. Trans.*, 2008, **36**, 1262–1266.
7 J. Y. Uriu-Adams and C. L. Keen, *Birth Defects Res., Part B*, 2010, **89**, 313–325.
8 B. Szewczyk, *Front. Aging Neurosci.*, 2013, **5**, 1–12.
9 B. L. Mihelich, E. A. Khramtsova, N. Arva, A. Vaishnav, D. N. Johnson, A. A. Giangreco, E. Martens-Uzunova, O. Bagasra, A. Kajdacsy-Balla and L. Nonn, *J. Biol. Chem.*, 2011, **286**, 44503–44511.
10 L. Y. Fong, R. Jing, K. J. Smalley, Z.-X. Wang, C. Taccioli, S. Fan, H. Chen, H. Alder, K. Huebner, J. L. Farber, O. Fiehn and C. M. Croce, *Proc. Natl. Acad. Sci. U. S. A.*, 2018, **115**, E11091–E11100.
11 Q. Sun, R. M. Van Dam, W. C. Willett and F. B. Hu, *Diabetes Care*, 2009, **32**, 629–634.
12 C. W. Shuttleworth and J. H. Weiss, *Trends Pharmacol. Sci.*, 2011, **32**, 480–486.
13 S. J. Lippard and E. Tomat, *Curr. Opin. Chem. Biol.*, 2010, **14**, 225–230.
14 Q. Lu, H. Haragopal, K. G. Slepchenko, C. Stork and Y. V. Li, *Int. J. Physiol., Pathophysiol. Pharmacol.*, 2016, **8**, 35–43.
15 C. D. Ellis, F. Wang, C. W. MacDiarmid, S. Clark, T. Lyons and D. J. Eide, *J. Cell Biol.*, 2004, **166**, 325–335.
16 M.-H. Kim, T. B. Aydemir, J. Kim and R. J. Cousins, *Proc. Natl. Acad. Sci. U. S. A.*, 2017, **114**, E5805–E5814.
17 B. H. Bin, J. Bhin, J. Seo, S. Y. Kim, E. Lee, K. Park, D. H. Choi, T. Takagishi, T. Hara, D. Hwang, H. Koseki, Y. Asada, S. Shimoda, K. Mishima and T. Fukada, *J. Invest. Dermatol.*, 2017, **137**, 1682–1691.
18 S. L. Sensi, D. Ton-That, P. G. Sullivan, E. A. Jonas, K. R. Gee, L. K. Kaczmarek and J. H. Weiss, *Proc. Natl. Acad. Sci. U. S. A.*, 2003, **100**, 6157–6162.
19 A. Atkinson, O. Khalimonchuk, P. Smith, H. Sabic, D. Eide and D. R. Winge, *J. Biol. Chem.*, 2010, **285**, 19450–19459.

20 G. Zhang, M. Sheng, J. Wang, T. Teng, Y. Sun, Q. Yang and Z. Xu, *J. Mol. Cell. Cardiol.*, 2018, **118**, 169–182.
21 J. J. Hwang, S.-J. Lee, T.-Y. Kim, J.-H. Cho and J.-Y. Koh, *J. Neurosci.*, 2008, **28**, 3114–3122.
22 H. C. Roh, S. Collier, J. Guthrie, J. D. Robertson and K. Kornfeld, *Cell Metab.*, 2012, **15**, 88–99.
23 D. Wu, A. C. Sedgwick, T. Gunnlaugsson, E. U. Akkaya, J. Yoon and T. D. James, *Chem. Soc. Rev.*, 2017, **46**, 7105–7123.
24 Y. Chen, Y. Bai, Z. Han, W. He and Z. Guo, *Chem. Soc. Rev.*, 2015, **44**, 4517–4546.
25 M. H. Lee, J. S. Kim and J. L. Sessler, *Chem. Soc. Rev.*, 2015, **44**, 4185–4191.
26 H. M. Kim and B. R. Cho, *Chem. Rev.*, 2015, **115**, 5014–5055.
27 L. Yuan, W. Lin, K. Zheng and S. Zhu, *Acc. Chem. Res.*, 2013, **46**, 1462–1473.
28 S. Iyoshi, M. Taki and Y. Yamamoto, *Org. Lett.*, 2011, **13**, 4558–4561.
29 D. Li, S. Chen, E. A. Bellomo, A. I. Tarasov, C. Kaut, G. A. Rutter and W.-H. Li, *Proc. Natl. Acad. Sci. U. S. A.*, 2011, **108**, 21063–21068.
30 R. J. Radford, W. Chyan and S. J. Lippard, *Chem. Sci.*, 2013, **4**, 3080–3084.
31 K. Rathore, C. S. Lim, Y. Lee, H. J. Park and B. R. Cho, *Asian J. Org. Chem.*, 2014, **3**, 1070–1073.
32 H. M. Kim, C. S. Lim, G. Masanta, H. J. Kim, B. R. Cho and J. H. Han, *J. Am. Chem. Soc.*, 2011, **133**, 5698–5700.
33 Z. Guo, Z. Liu, W. He, C. Zhang and Y. Chen, *Chem. Commun.*, 2012, **48**, 8365.
34 L. Xue, G. Li, C. Yu and H. Jiang, *Chem. – Eur. J.*, 2012, **18**, 1050–1054.
35 W. Chyan, D. Y. Zhang, S. J. Lippard and R. J. Radford, *Proc. Natl. Acad. Sci. U. S. A.*, 2014, **111**, 143–148.
36 Q. Liu, D. Zhu, H. Jiang, L. Xue and G. Li, *Inorg. Chem.*, 2012, **51**, 10842–10849.
37 H. Zhu, J. Fan, S. Zhang, J. Cao, K. Song, D. Ge, H. Dong, J. Wang and X. Peng, *Biomater. Sci.*, 2014, **2**, 89–97.
38 H. J. Lee, C. W. Cho, H. Seo, S. Singha, Y. W. Jun, K. H. Lee, Y. Jung, K. T. Kim, S. Park, S. C. Bae and K. H. Ahn, *Chem. Commun.*, 2016, **52**, 124–127.
39 C. Du, S. Fu, X. Wang, A. C. Sedgwick, W. Zhen, M. Li, X. Li, J. Zhou, Z. Wang, H. Wang and J. L. Sessler, *Chem. Sci.*, 2019, **10**, 5699–5704.
40 X. Gan, P. Sun, H. Li, X. Tian, B. Zhang, J. Wu, Y. Tian and H. Zhou, *Biosens. Bioelectron.*, 2016, **86**, 393–397.
41 W. Lin, D. Buccella and S. J. Lippard, *J. Am. Chem. Soc.*, 2013, **135**, 13512–13520.
42 S. J. Lippard, E. Tomat, E. M. Nolan and J. Jaworski, *J. Am. Chem. Soc.*, 2008, **130**, 15776–15777.
43 H. Singh, H. W. Lee, C. H. Heo, J. W. Byun, A. R. Sarkar and H. M. Kim, *Chem. Commun.*, 2015, **51**, 12099–12102.
44 H. M. Kim, B. R. Cho, G. Masanta, C. S. Lim, C. H. Heo and N. Y. Baek, *Chem. Commun.*, 2012, **48**, 4546.
45 Z. Liu, C. Zhang, Y. Chen, W. He and Z. Guo, *Chem. Commun.*, 2012, **48**, 8365–8367.
46 X. Xie, F. Tang, X. Shangguan, S. Che, J. Niu, Y. Xiao, X. Wang and B. Tang, *Chem. Commun.*, 2017, **53**, 6520–6523.
47 H. Xiao, P. Li, X. Hu, X. Shi, W. Zhang and B. Tang, *Chem. Sci.*, 2016, **7**, 6153–6159.
48 M. Yang, J. Fan, J. Zhang, J. Du and X. Peng, *Chem. Sci.*, 2018, **9**, 6758–6764.
49 J.-T. Hou, H. S. Kim, C. Duan, M. S. Ji, S. Wang, L. Zeng, W. Ren and J. S. Kim, *Chem. Commun.*, 2019, 2533–2536.
50 W. Lin, G. Xu, S. Gao, Y. Ma, Y. Tang and A. Xu, *Sci. Rep.*, 2017, **7**, 1–9.
51 J. Pancholi, D. J. Hodson, K. Jobe, G. A. Rutter, S. M. Goldup and M. Watkinson, *Chem. Sci.*, 2014, **5**, 3528–3535.
52 L. Fang, G. Trigiante, C. J. Kousseff, R. Crespo-Otero, M. P. Philpott and M. Watkinson, *Chem. Commun.*, 2018, **54**, 9619–9622.
53 E. Calatrava-Pérez, S. A. Bright, S. Achermann, C. Moylan, M. O. Senge, E. B. Veale, D. C. Williams, T. Gunnlaugsson and E. M. Scanlan, *Chem. Commun.*, 2016, **52**, 13086–13089.
54 E. Calatrava-Pérez, J. M. Delente, S. Shanmugaraju, C. S. Hawes, C. D. Williams, T. Gunnlaugsson and E. M. Scanlan, *Org. Biomol. Chem.*, 2019, **17**, 2116–2125.
55 A. K. Bandela, S. Bandaru and C. Pulla, *Chem. – Eur. J.*, 2015, **21**, 13364–13374.
56 J. Chaignon, S. E. Stiriba, F. Lloret, C. Yuste, G. Pilet, L. Bonneviot, B. Albela and I. Castro, *Dalton Trans.*, 2014, **43**, 9704–9713.
57 A. Hayata, H. Itoh, S. Matsutaka and M. Inoue, *Chem. – Eur. J.*, 2016, **22**, 3370–3377.
58 K. Jobe, C. H. Brennan, M. Motevalli, S. M. Goldup and M. Watkinson, *Chem. Commun.*, 2011, **47**, 6036–6038.
59 T. N. Tomoya Hirano, K. Kikuchi, Y. Urano and T. Higuchi, *J. Am. Chem. Soc.*, 2000, **122**, 12399–12400.
60 M. Shortreed, R. Kopelman, M. Kuhn and B. Hoyland, *Anal. Chem.*, 1996, **68**, 1414–1418.
61 W. Lin, L. Long and W. Tan, *Chem. Commun.*, 2010, **46**, 1503–1505.
62 E. B. Veale and T. Gunnlaugsson, *J. Org. Chem.*, 2008, **73**, 8073–8076.
63 E. Tamanini, A. Katewa, L. M. Sedger, M. H. Todd and M. Watkinson, *Inorg. Chem.*, 2009, **48**, 319–324.
64 E. Tamanini, K. Flavin, M. Motevalli, S. Piperno, L. A. Gheber, M. H. Todd and M. Watkinson, *Inorg. Chem.*, 2010, **49**, 3789–3800.
65 L. Fang, G. Trigiante, R. Crespo-Otero, C. S. Hawes, M. P. Philpott, C. R. Jones and M. Watkinson, *Chem. Sci.*, submitted for publication.
66 H. Su, X. Chen and W. Fang, *Anal. Chem.*, 2014, **86**, 891–899.
67 D. Escudero, *Acc. Chem. Res.*, 2016, **49**, 1816–1824.